

# Journal of Mechanics of Materials and Structures

**AN ASYMPTOTIC METHOD FOR THE PREDICTION  
OF THE ANISOTROPIC EFFECTIVE ELASTIC PROPERTIES  
OF THE CORTICAL VEIN: SUPERIOR SAGITTAL SINUS JUNCTION  
EMBEDDED WITHIN A HOMOGENIZED CELL ELEMENT**

Rania Abdel Rahman, Daniel George, Daniel Baumgartner, Mathieu Nierenberger,  
Yves Rémond and Saïd Ahzi

Volume 7, No. 6

June 2012



mathematical sciences publishers

# AN ASYMPTOTIC METHOD FOR THE PREDICTION OF THE ANISOTROPIC EFFECTIVE ELASTIC PROPERTIES OF THE CORTICAL VEIN: SUPERIOR SAGITTAL SINUS JUNCTION EMBEDDED WITHIN A HOMOGENIZED CELL ELEMENT

RANIA ABDEL RAHMAN, DANIEL GEORGE, DANIEL BAUMGARTNER,  
MATHIEU NIERENBERGER, YVES RÉMOND AND SAÏD AHZI

Bridging veins (BVs) are frequently damaged in traumatic brain injury due to brain-skull relative motion. These veins, connected to the superior sagittal sinus (SSS), are prone to rupture upon head impact giving rise to an acute subdural hematoma (ASDH). We modeled the biomechanical characteristics of ASDH to study the behavior of the SSS-BVs compound with its surrounding medium. The almost periodic distribution of the BVs along the SSS allowed the use of the homogenization method based on asymptotic expansion to calculate the effective elastic properties of the brain-skull interface region. The representative volume element (RVE) under study is an anisotropic equivalent medium with homogenized elastic properties, accounting for the variations of each constituent's mechanical properties. It includes the sinus, the BVs and blood, and the surrounding cerebrospinal fluid and tissue. The results show large variations in the RVE anisotropic properties depending on each constituent of the BV and, to a certain extent, on the variability of the surrounding constituents' mechanical properties.

## 1. Introduction

Acute subdural hematoma (ASDH) is a potentially devastating, yet curable extra-axial fluid collection within the potential subdural space. It is classically associated with head trauma rising from rapid acceleration and/or deceleration that produces the rupture of cortical arteries and most often occurs by tearing of bridging veins (BVs) as they cross from the brain surface to the dural sinus [Maxeiner and Wolff 2002]. Fenderson et al. [2007] reported that these veins are prone to rupture at the point of their entry into the SSS, and this was confirmed by the results of microscopy examination [Yamashima and Friede 1984; Vignes et al. 2007]. They found that, due to the histological composition of the BVs and the change in the collagen pattern in the vein walls near their entrance into the superior sagittal sinus (SSS), the subdural portion of a BV is more fragile than its subarachnoidal portion. The rupture of BVs is induced by the brain-skull relative motion following a head impact as described by neuropathologists [Yamashima and Friede 1984] and by experimental work conducted in vivo [Willinger et al. 1995; Ji et al. 2004; Bayly et al. 2005; Ji and Margulies 2007; Sabet et al. 2008].

The motion between the brain and the skull has been considered potentially important to head injury. In order to evaluate this potential problem, finite element (FE) modeling of the human head was developed to evaluate the brain-skull interface conditions [Kleiven and Hardy 2002; Wittek and Omeri 2003]. An important issue in the numerical analysis is the selection of material properties. While there

*Keywords:* homogenization, mechanical behavior, bridging veins, brain-skull interface, elastic properties, biological material.

are several macroscopic FE models of the human head, only one local 3D FE model has been developed, by [Moghadam and Sadegh \[2009\]](#), to study the details of the brain-skull interface region to analyze the rupture of BVs. The use of classical finite element methods to find the local behavior at each point of a complicated biological structure such as the brain-skull interface region is very difficult. Thus, the use of homogenization methods at different scales is becoming unavoidable. Different authors have used multiscale approaches [[Sanz-Herrera et al. 2009](#); [Bertaud et al. 2010](#); [Soliman et al. 2010](#)] to define the mechanical behavior of biological tissue. The finite element approach has been adopted by [Karami et al. \[2009\]](#) to analyze the homogenized mechanical response of brain white matter under large deformation. [Yoon et al. \[2002\]](#) estimated the effective transversely isotropic elastic constants of bones from orthotropic data found in the literature. The aim of the present work is to analytically determine the homogenized mechanical properties of the segment representing the junction between the SSS, the BV, and the surrounding constituents. This zone will be considered as a heterogeneous medium which will be transformed to a mechanically equivalent medium (effective medium) that is anisotropic and homogeneous. In turn, this equivalent medium can be incorporated as a heterogeneous element in a macroscopic model, such as FEM.

The calculations are conducted on a representative volume element (RVE) of the size order of the BV. To achieve this goal, the anatomy, the geometrical arrangement, and the mechanical properties of the tissues forming the investigated segment must be adequately defined. In addition, in order to be able to include this analysis in a macroscopic model of the head, the geometry and size of the RVE should be able to fulfill the following two requirements: first, have a similar size and geometry as the local geometrical element present in the macroscopic model, and second, be able to take into account the local microscopic heterogeneous medium of the BV and surroundings in order to provide an accurate anisotropic heterogeneous behavior. These constraints are strong and influence the results of the analysis. Nevertheless, this work will enable us to make a first evaluation of the elastic behavior of BVs, which is carried out on the local level using a micromechanical approach. This paper presents the geometrical model development together with theoretical analysis. The results are given for the anisotropic behavior of the RVE at the macroscopic scale. The variations of these results are discussed as a function of the local constituents' behavior and the surrounding environment.

## 2. Materials description

**2.1. Geometry localization and material properties.** [Figure 1](#) shows the distribution and positioning of the anisotropic RVE along the SSS in order to take into account the BVs' specific behavior. We assumed that the homogenized cell follows the SSS main axis with a perpendicular BV attached to it. This cell will represent the RVE for which the homogenization method will be applied.

It is always difficult to precisely characterize the mechanical response of biological tissue and especially soft tissue. The local geometries and material properties for the RVE's local constituent were extracted from [[Yamashima and Friede 1984](#); [Lee and Haut 1989](#); [Henrikson et al. 1997](#); [Kleiven 2002](#); [Bashkatov et al. 2003](#); [Horgan 2005](#)] for the dimensions and [[Melvin et al. 1970](#); [Ruan et al. 1993](#); [Huang et al. 1999](#); [Willinger et al. 1999](#); [Monson et al. 2005](#)] for the mechanical properties. All the materials in the current study were supposed linear elastic in a first approximation. The chosen geometry and corresponding mechanical properties for the SSS and BVs are presented in [Table 1](#). In this table,

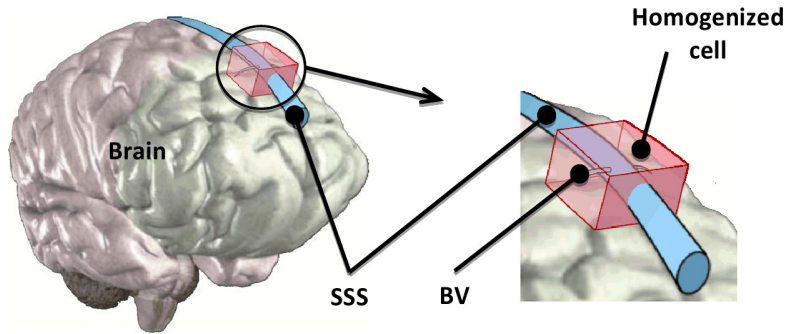


**Figure 1.** Schematic positioning of the anisotropic RVE as a part of the macroscopic model of the head.

$E_l$  and  $E_t$  represent the longitudinal (relative to the BV’s main axis) and transverse Young’s moduli, respectively, and  $\nu_{lt}$  and  $\nu_{tl}$  are the corresponding Poisson’s coefficients. Apart from the wall thickness and diameter of the blood vessels, other dimensions are irrelevant in our study since they depend on the size of the used homogenized cell and are accounted for in the homogenization method.

Some work was carried out on the brain and surrounding tissue such as in [Pham and Sun 2010; Prevost et al. 2011a; 2011b]. In these works, the investigated volume represents the brain-skull interface region (BSIR) in the zone of the junction of the BVs with the SSS walls. This volume is a complex zone mostly filled with liquid and comprises the sinus, the bridging veins, the blood circulating inside them, and the surrounding cerebrospinal fluid and tissues. An experimental study using modal analysis of the head in vivo was conducted by Willinger and Césari [1990; 1995; 1999] on the dynamic behavior of the brain-skull interface. This study was based on a hammer impact method on the head. It showed that for so-called long shocks in the range 0.012 to 0.025 ms, the shock spectrum energy is distributed in a frequency range below 150 Hz and the brain follows the movement of the head. On the contrary, for so-called short impacts in the range 0.004 to 0.012 ms, the shock spectrum is distributed in a frequency range above 150 Hz, the brain no longer follows the skull movement, and relative displacement occurs between the brain and the skull. This experimental work coupled with an FEM modal analysis using springs and dashpots based on rheological models enabled the evaluation of an equivalent stiffness of the BSIR zone, which was 0.012 MPa. It appears to be of the same order as the average stiffness values of the brain, measured between 0.07 MPa and 0.675 MPa [Ruan et al. 1991; Willinger et al. 1992; Kumaresan and Radhakrishnan 1996; Ruan and Prasad 1996; Sarkar et al. 2004]. However it is much smaller than the stiffness value of the skull, measured at 15 GPa for parietal bone and 4 GPa for the diploë [Willinger et al. 1999;

Tissue	Geometry (mm)	Mechanical properties	
		Young’s modulus, $E$ (MPa)	Poisson’s ratio, $\nu$
SSS	Wall thickness = 0.5	31.5	0.45
BVs	Diameter = 1.5	$E_l = 6.43$	$\nu_{lt} = 0.385$
	Wall thickness = 0.25	$E_t = 2.4$	$\nu_{tl} = 0.49$

**Table 1.** Geometry and mechanical properties of the studied tissues.

Ho and Kleiven 2007; Yao et al. 2008; Yu et al. 2008]. In the current work, we used this measured value (0.012 MPa) in our mechanical analysis for the BSIR and, in order to be consistent with a fluid-like mechanical behavior, we allocated a Poisson's ratio of 0.49. The thickness of the BSIR included in the RVE was 1.5 mm. The mechanical behavior of the blood inside the BVs poses a similar problem as the mechanical behavior of the BSIR between the brain and skull, although it is enclosed within the BVs' or SSS's walls. However, the BVs' walls are of different stiffness than those of the brain and skull. Therefore, the stiffness response of the blood inside the BVs is different from its response between the brain and skull. In order to take this into account in our analysis, we made a parametric study of the influence of blood properties on the overall mechanical behavior of the RVE. This will be presented in the results section.

The average reported viscosity of the blood ( $\mu_{bl,av} = 0.004 \text{ Pa}\cdot\text{s}$  [Chatziprodromou et al. 2007; Li et al. 2007]) is situated in between that of water ( $\mu_{water} = 0.001 \text{ Pa}\cdot\text{s}$ ) and that of the BSIR ( $\mu_{BSIR} = 0.0085 \text{ Pa}\cdot\text{s}$  [Bloomfield et al. 1998]). For an average strain rate under the given loading conditions of about  $10 \text{ s}^{-1}$  for the BVs (depending on their length and loading time), the stresses developed due to viscosity are very small (typically of the order of 0.01 Pa) compared to other stresses developed by the harder materials of the RVE under the same mechanical loads. Therefore we can assume that the stresses developed by the viscosity of the blood inside the RVE will be of the same order of magnitude as that of the BSIR at the brain-skull interface. In the current work, the studied range of blood properties was varied between 0.012 MPa (equivalent to that of the BSIR from Willinger and Césari [1990; 1995; 1999]) and 1 MPa, which is about half the stiffness value of the BV walls. We believe this range of study is large enough to validate our model and determine accurately the anisotropic behavior of the RVE in the range of the applied mechanical loads. For convenience, we named the equivalent stiffness of the blood ( $K_{bl}$ ) and in the same way as for the BSIR mechanical characteristics, we allocated a Poisson's ratio of 0.49. Finally, the value of the elastic modulus of the SSS ( $E_s$ ) was varied from 30 to 60 MPa. These values were extracted from [Delye et al. 2006; Mukherjee et al. 2006] to cover an average range of values cited in the literature. The effect of variations in these parameters on the values of the RVE homogenized elasticity coefficients was also determined and is presented in the results section.

The BV was treated as an orthotropic material composed of collagen fibers of Young's modulus ( $E_c$ ) = 1 GPa surrounded by a matrix formed of elastin of Young's modulus ( $E_e$ ) = 0.6 MPa, as mentioned in [Park and Lakes 2007]. The collagen to elastin ratio was considered to be 3:1 as reported in [Samet and Lelkes 1999]. The transverse elastic modulus ( $E_t$ ) and transverse Poisson's ratio ( $\nu_{tt}$ ) were calculated by considering a lower bound approach using a simple Reuss averaging scheme while the longitudinal elastic modulus ( $E_l$ ) was chosen from [Monson et al. 2005]. The longitudinal Poisson's ratio ( $\nu_{lt}$ ) was obtained from the standard rule of mixture. Table 2 summarizes the elastic mechanical properties of the BV. In our analyses, the properties of the BV itself are kept constant since they are directly taken from data from the literature. Some patient-dependant variations are to be expected but it is believed that they will not influence greatly the anisotropic behavior of the considered RVE in this simple case. The muscle strength in the BVs was not taken into account in this work since their rigidity is very small (there are

Property	$E_l$ (MPa)	$E_t$ (MPa)	$\nu_{lt}$	$\nu_{tt}$	$G_{lt}$ (MPa)	$G_{tt}$ (MPa)
Value	6.43	2.4	0.385	0.49	0.8	0.8

**Table 2.** Elastic mechanical properties of the BV.

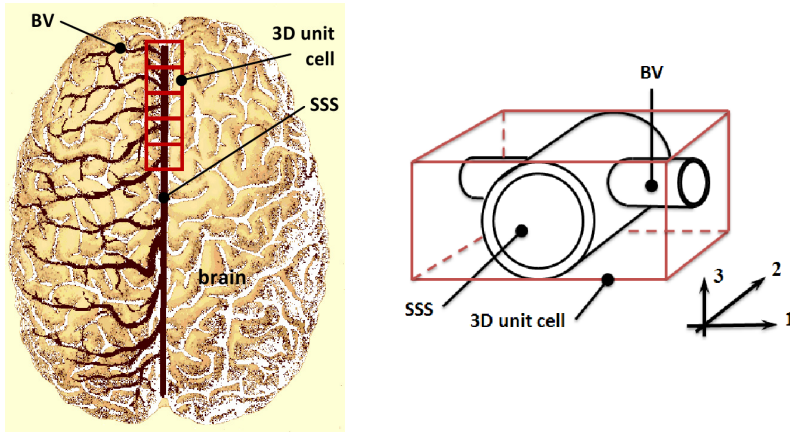


**Figure 2.** Left: distribution of BVs along the SSS as shown in [Rhoton 2002]. Right: a schematic of the RVE on the SSS-BV junction.

almost no muscles in the BVs due to their location and size). Therefore, the muscles have a negligible impact on the BVs’ mechanical behavior compared to the rigidity of the collagen and elastin fibers.

The RVE is therefore composed of SSS, BV, blood, and BSIR components for which all mechanical characteristics are defined. Other tissues are not taken into account in this analysis since they are supposed to be outside the RVE.

**2.2. Periodicity problem.** BVs are fairly symmetrically distributed on both sides of the SSS and evenly distributed along the axis of the sinus in the sagittal plane as shown in Figure 2, left. Therefore we considered the distribution of BVs to be almost periodic in the sagittal direction and we applied the homogenization method based on the asymptotic expansion.

Figure 2, right, illustrates the SSS-BV junction. As explained previously, the investigation zone is defined as a geometrical 3D unit cell. This unit cell was chosen to be the representative volume element (RVE) used in the current micro-meso homogenization calculations. Note that the symmetrical distribution (or not) of the BVs on each side of the SSS is not relevant here since this is automatically taken into account in the asymptotic homogenization process.

### 3. Homogenization method by asymptotic expansion

**3.1. Theory.** We will present here the main steps of the method. Let  $L$  represent the characteristic dimension of the overall structure, then  $\eta L$  will define the size of the RVE. We denote by  $X$  the slow variable reflecting the variation in the magnitude of the properties at the structure scale and by  $Y$  the local variable describing the rapid variation on the RVE. Thus,  $X$  and  $Y$  are related together through

$$\eta = \frac{X}{Y}. \tag{1}$$

If  $\vec{U}(X, Y)$  is the displacement field, it may be expressed in terms of infinite expansion series, as proposed in [Sanchez-Palencia 1974; Ladeveze et al. 1985; Dumont et al. 1987; Devries et al. 1989]:

$$\vec{U}(X, Y) = \vec{U}_0(X, Y) + \eta \vec{U}_1(X, Y) + \eta^2 \vec{U}_2(X, Y) + \dots \tag{2}$$

The elastic deformation written here in small deformations is decomposed as a function of slow and rapid variables (it can be developed for large deformation):

$$\epsilon_{ij} = \epsilon_{xij} + \frac{1}{\eta} \epsilon_{yij}, \tag{3}$$

where  $\epsilon_x$  and  $\epsilon_y$  are the strain tensors corresponding to the slow and rapid variables, respectively. Knowing that  $\sigma = K\epsilon$  (Hooke’s law), the stress differential operator  $\text{div } \sigma(X, Y)$  may be written as follows:

$$\text{div } K\epsilon = \text{div}_x K\epsilon + \frac{1}{\eta} \text{div}_y K\epsilon, \tag{4}$$

where  $K$  represents the local elastic properties and  $\text{div}_x$  and  $\text{div}_y$  are the divergence operators corresponding to slow and rapid variables, respectively.

The equilibrium equation of the periodic medium is  $\text{div } \sigma(X, Y) + f = 0$  where  $f$  is the volume force. It induces

$$\text{div}_y K\epsilon_y(\vec{U}_0) = 0, \tag{5}$$

$$\text{div}_y K\epsilon_y(\vec{U}_1) + \text{div}_y K\epsilon_x(\vec{U}_0) + \text{div}_x K\epsilon_y(\vec{U}_0) = 0, \tag{6}$$

$$\text{div}_y K\epsilon_y(\vec{U}_2) + \text{div}_y K\epsilon_x(\vec{U}_1) + \text{div}_x K\epsilon_y(\vec{U}_1) + \text{div}_x K\epsilon_x(\vec{U}_0) + f = 0. \tag{7}$$

Solving (5), (6), and (7) gives  $\vec{U}_0, \vec{U}_1,$  and  $\vec{U}_2,$  which are the solutions of the following variational formulation:

$$\text{Find } \vec{\vartheta} \in \vartheta_{\text{per}} / \forall \vec{\vartheta}^* \in \vartheta_{\text{per}}, \int_M \text{Tr}[K\epsilon_y(\vec{\vartheta})\epsilon_y(\vec{\vartheta}^*)] d\Omega = \int_M \vec{g} \cdot \vec{\vartheta}^* d\vec{\Omega}, \tag{8}$$

with  $\vec{g} = -\text{div}[K.\epsilon_y(\vec{U})]$  and  $\vartheta_{\text{per}} = \vec{U} / U^+ = U^-$ , where  $U^+$  and  $U^-$  represent the values of  $\vec{U}$  on 2 opposite faces of the RVE and are equal.  $M$  represents the unit cell (RVE) and  $\int_{M^*} d\vec{\Omega} = V^*$ , where  $V^*$  is the volume of the RVE. For more details, see [Mahmoud 2010, pp. 44–65].

From the solution of (5), (6), and (7) it can be concluded that

- $\vec{U}_0$  depends only on  $X$ :  $\vec{U}_0 = \vec{U}_0(X)$ .
- $\vec{U}_0$  and  $\vec{U}_1$  are linearly dependent since

$$K_{ijkl}\epsilon_{ykl}(\vec{U}_1) = H_{ijkl}\epsilon_{xkl}(\vec{U}_0) \tag{9}$$

where  $H$  is a symmetric linear operator.

The equilibrium equation of the periodic medium becomes

$$\text{div}_x \int_M [(H + K)\epsilon_x(\vec{U}_0)] d\Omega + f \int_M d\Omega = 0. \tag{10}$$

Note that  $\vec{U}_0$  represents the homogenized displacement over the RVE while  $\vec{U}_1$  represents the perturbation of the displacement.

Finally, using the macroscopic (RVE) Hooke’s law  $\sigma^* = K^*\epsilon^*$ , relating the macroscopic stress tensor  $\sigma^*$  to the macroscopic elastic strain tensor  $\epsilon^*$ , along with (9) and (10) we get the homogenized behavior of the periodic medium. This leads to the following expression of the effective elastic stiffness tensor  $K^*$ :

$$K^*_{ijkl} = \frac{1}{\text{vol}(M)} \int_M (H_{ijkl} + K_{ijkl}) dM. \tag{11}$$

Moreover, we can express the problem in  $\vec{U}_1$  as follows:

$$\vec{U} \rightarrow \frac{1}{2} \int_M K_{ijkl} \epsilon_{yij}(\vec{U}) \epsilon_{ykl}(\vec{U}) dM + \int_M K_{ijkl} \epsilon_{xij}(\vec{U}_0) \epsilon_{ykl}(\vec{U}) dM. \tag{12}$$

Knowing that  $\epsilon_y(\vec{U}_1)$  and  $\epsilon_x(\vec{U}_0)$  are linearly dependent as shown in relation (9), we have  $\vec{U}_1 = A_{rs} \epsilon_{rs}(\vec{U}_0)$  with  $A_{rs} \in W(M)$ . Thus the variational problem (12) is now as follows.

Find  $A_{rs} \in W(M)$  by minimizing the following functions:

$$U \rightarrow \frac{1}{2} \int_M K_{ijkl} \epsilon_{yij}(\vec{U}) \epsilon_{ykl}(\vec{U}) dM + \int_M K_{rskl} \epsilon_{xij}(\vec{U}_0) \epsilon_{ykl}(\vec{U}) dM, \tag{13}$$

$$K_{ijkl}^* = \frac{1}{\text{vol}(M)} \int_M [K_{ijrs} + K_{ijkl} \epsilon_{kl}(\vec{U})] dM. \tag{14}$$

Here  $W(M)$  is the displacement space, and  $(r, s)$  equals  $(1, 1)$ ,  $(2, 2)$ , and  $(3, 3)$  in the case of normal loading and  $(1, 2)$ ,  $(2, 3)$ , and  $(3, 1)$  in the case of shear loading.

**3.2. Application to the representative volume element.** Since the basic unit cell (RVE) is symmetric about the three orthogonal planes, we can develop the theory only on an eighth of the RVE. By making this simplification we assume that the periodicity is present in all directions, which is not the real case. This assumption can be justified since the results of the homogenization done in the current study were applied to estimate the global and local behaviors of the constituents of the brain-skull interface region only in the case of sagittal impacts. The anatomical periodicity being in the sagittal plane, the previous assumption is valid since no influence will be developed in other directions. In addition, the principle of our calculations is linear. It is simply transposed to the curvilinear structure of the head.

The different loading cases can be dissociated and the relations (13) and (14) are minimized on

$$W_0(M) = \{ \vec{U} / U_1 = 0|_{0,L_1}; U_2 = 0|_{0,L_2}; U_3 = 0|_{0,L_3} \} \quad \text{for } r, s = (1, 1), (2, 2), (3, 3), \tag{15}$$

$$W_1(M) = \{ \vec{U} / U_1 = 0|_{0,L_1}; U_1 = U_3 = 0|_{0,L_2}; U_1 = U_2 = 0|_{0,L_3} \} \quad \text{for } r, s = (2, 3), \tag{16}$$

$$W_2(M) = \{ \vec{U} / U_2 = U_3 = 0|_{0,L_1}; U_2 = 0|_{0,L_2}; U_1 = U_2 = 0|_{0,L_3} \} \quad \text{for } r, s = (3, 1), \tag{17}$$

$$W_3(M) = \{ \vec{U} / U_2 = U_3 = 0|_{0,L_1}; U_1 = U_3 = 0|_{0,L_2}; U_3 = 0|_{0,L_3} \} \quad \text{for } r, s = (1, 2). \tag{18}$$

To find the homogenized coefficients, the eighth of the RVE takes into account each single constituent individually by subdividing the RVE into smaller parts. The loading cases were treated separately and applied on the unit cell as follows:

- A displacement condition was used in the case of normal load because the strain remains almost constant in this case.
- The stresses being quasiuniform with shear loading, they were applied to find the lower limit values of the shear components for the effective elastic stiffness. Then, a weighting approach between the stress applied and the rule of mixture was used to find the average values of the upper and lower limits of these coefficients.

*Description of the displacement field loading condition.* First we treated the case of displacement field  $\vec{U}$  affine per part and continuous in normal loading situations in the space  $W_0(M)$  and we got the values of  $K_{ijkl}^*$  where  $i = j$ . The associated deformation field is constant per part.

The problem in  $\vec{U}_1$  was resolved by minimizing the relation (15) over  $W_0(M)$ . For the case of  $r, s = (1, 1)$  the problem in  $\vec{U}_1$  was written as follows:

$$\sum_{i=1}^8 \int_i \{ (K_{11}\epsilon_{11} + K_{12}\epsilon_{22} + K_{13}\epsilon_{33})\epsilon_{11}^* + (K_{12}\epsilon_{11} + K_{22}\epsilon_{22} + K_{23}\epsilon_{33})\epsilon_{22}^* + (K_{13}\epsilon_{11} + K_{23}\epsilon_{22} + K_{33}\epsilon_{33})\epsilon_{33}^* + (K_{11}\epsilon_{11}^* + K_{12}\epsilon_{22}^* + K_{13}\epsilon_{33}^*)dV_i \} = 0, \quad \forall \epsilon_{11}^*, \epsilon_{22}^*, \epsilon_{33}^* \in W_0(M). \quad (19)$$

Replacing  $K$  by the characteristics of the tissues existing in each portion and by isolating the terms associated with  $\epsilon_{11}^*, \epsilon_{22}^*$ , and  $\epsilon_{33}^*$ , we found a system of three equations as a function of the strain supposed constant per part.

The homogenized coefficients  $K_{11}^*, K_{21}^*$ , and  $K_{31}^*$ , were calculated from the relation (14) for  $r, s = (1, 1)$  as follows:

$$K_{11}^* = \frac{1}{\text{vol}(M)} \int_M [K_{11} + K_{11}\epsilon_{11} + K_{12}\epsilon_{22} + K_{13}\epsilon_{33}]dM, \quad (20)$$

$$K_{21}^* = \frac{1}{\text{vol}(M)} \int_M [K_{21} + K_{21}\epsilon_{11} + K_{22}\epsilon_{22} + K_{23}\epsilon_{33}]dM, \quad (21)$$

$$K_{31}^* = \frac{1}{\text{vol}(M)} \int_M [K_{31} + K_{31}\epsilon_{11} + K_{32}\epsilon_{22} + K_{33}\epsilon_{33}]dM. \quad (22)$$

By a summation over all the subdivided parts of the RVE, we obtained the values of  $K_{11}^*, K_{21}^*$ , and  $K_{31}^*$ . The same procedure was repeated for the cases of  $r, s = (2, 2)$  and  $r, s = (3, 3)$  to evaluate the values of  $K_{22}^*, K_{12}^*, K_{32}^*, K_{33}^*, K_{13}^*$ , and  $K_{23}^*$ .

*Description of the stress field loading condition.* To find the lower limits of the shear coefficients, we used the duality on the displacement spaces. The dual stress formulation is as follows.

Find  $\bar{\sigma} \in W^*(M)$ , by minimizing the form

$$\frac{1}{2} \int_M \text{Tr}[\bar{\sigma} K^{-1} \bar{\sigma}]dM + \int_M \text{Tr}[\epsilon(U_0)\bar{\sigma}]dM, \quad (23)$$

where  $W^*(M)$  are the spaces for statically admissible stress fields.

The spaces  $W_i(M), i = 1, 2, 3$ , become:

$$W_1^*(M) = \{ \sigma / \sigma_{12} = \sigma_{13} = 0|_{0,L_1}; \sigma_{22} = 0|_{0,L_2}; \sigma_{33} = 0|_{0,L_3} \}, \quad (24)$$

$$W_2^*(M) = \{ \sigma / \sigma_{11} = 0|_{0,L_1}; \sigma_{21} = \sigma_{23} = 0|_{0,L_2}; \sigma_{33} = 0|_{0,L_3} \}, \quad (25)$$

$$W_3^*(M) = \{ \sigma / \sigma_{11} = 0|_{0,L_1}; \sigma_{22} = 0|_{0,L_2}; \sigma_{31} = \sigma_{32} = 0|_{0,L_3} \}. \quad (26)$$

The stress field is statically admissible and is assumed to be constant by part and continuous on the interfaces between parts.

For the case of  $r, s = (2, 3)$ :

$$W_1^*(M) = \left\{ \frac{\sigma}{\sigma_{12}} = \sigma_{13} = 0|_{0,L_1}; \sigma_{22} = 0|_{0,L_2}; \sigma_{33} = 0|_{0,L_3} \right\}.$$

Thus, we have only  $\sigma_{11}$  continuous in direction 1  $\sigma_{23}$  continuous in directions 2 and 3.

The dual formulation is expressed as follows:

$$\sum_{i=1}^8 \left\{ \int_i \text{Tr}[\sigma K^{-1} \sigma^*] dM_i + \int_i \text{Tr}[\epsilon(\vec{U}_0) \sigma^*] dM_i \right\} = 0, \quad \forall \sigma^* \in W_1^*, \tag{27}$$

which is equivalent in this case to:

$$\int_M (\sigma K^{-1} \sigma^* - \sigma_{23}) dM = 0. \tag{28}$$

It is possible to solve the problem analytically and when partitioning the RVE into 64 subdivided elements (8 × 8) we obtained for the fairly simple case of  $K_{44}^*$ :

$$K_{44}^* = 2G_{23}^* = \frac{1}{\frac{3}{8} K_{44\text{BSIR}}^{-1} + \frac{1}{14.4} K_{44\text{BV}}^{-1} + \frac{1}{2.9} K_{44\text{bl}}^{-1} + \frac{1}{4.7} K_{44\text{SS}}^{-1}}. \tag{29}$$

$G^*$  is the homogenized shear coefficient. The  $K$  variables are the rigidities for the BSIR, BV, blood, and SSS respectively. The same procedure can be used to determine the other effective stiffness coefficients, and  $K_{55}^*$  and  $K_{66}^*$  can be obtained fairly easily. Solving the system of equations is more complex for the other coefficients but workable. An overview of the methodology is given in the [Appendix](#) to obtain the whole matrix of effective stiffness coefficients.

#### 4. Results and discussion

**4.1. Numerical results of the homogenization.** The described methodology enabled us to obtain the values of the homogenized properties of the periodic structure for the orthotropic RVE. Different cases were studied as a function of, firstly, the variability of the Young’s modulus and Poisson’s ratio for the SSS and, secondly, the parametric study of the variable blood response enclosed within the RVE. The material characteristics of the BVs and dura matter were kept constant using the values presented above. The four studied cases are presented in [Table 3](#). In this table, we used the word “stiffness” corresponding to the Young’s modulus in the case of the SSS material properties. However, in the case of blood, we understand stiffness as the equivalent stiffness measured by [Willinger and Césari \[1990; 1995; 1999\]](#) as mentioned above. The resulting homogenized stiffness coefficients of the RVE are presented in [Table 4](#) and the elastic moduli and Poisson’s ratios, obtained using the minimum and maximum values for the SSS and blood, are illustrated in [Table 5](#).

Tissue	Case 1		Case 2		Case 3		Case 4	
	$E$	$\nu$	$E$	$\nu$	$E$	$\nu$	$E$	$\nu$
SSS	31.5	0.45	31.5	0.45	60	0.45	60	0.45
	$K$	$\nu$	$K$	$\nu$	$K$	$\nu$	$K$	$\nu$
Blood	1	0.49	0.012	0.49	1	0.49	0.012	0.49

**Table 3.** Range of values tested for the SSS and blood. Young’s moduli,  $E$ , and equivalent stiffness,  $K$ , values are in MPa and Poisson’s ratios,  $\nu$ , are nondimensional.

When the macroscopic model is used, the local anisotropic properties of the SSS-BV junction are calculated and evaluation of a potential rupture strain of the BV is made. The advantage of using this approach is twofold: the macro-micro effect enables us to obtain the local constituents' behavior in a 3D macroscopic analysis and the micro/macro effect enables us to evaluate the influence of variability of the local phenomena for each local constituent on the 3D global behavior.

It can be noticed that the studied RVE is highly anisotropic. The anisotropy governing the tensile behavior of our structure is deduced from the large differences existing between the material properties. This is true for the Young's and shear moduli, but the Poisson's ratios are closer to each other. Since the definition of the RVE was derived using one-eighth symmetry (that is, it assumes periodic distributions in all three directions of space), it is not possible to assess the influence of the loading direction in a general loading case. But in the current study, this symmetry is not relevant for the calculation of the effective properties of the RVE since the loading direction is exclusively in the direction of the SSS main axis and using one-eighth symmetry enables us to use known boundary conditions. However, a uniaxial periodicity would definitely change the effective material response in a more random situation.

We believe that the herein obtained results for a uniaxial periodicity should be of the same order of magnitude (as a function of the parameters' variability) under other loading symmetries. However, it is necessary to develop a numerical model in order to accurately evaluate this influence.

Case 1	$\begin{pmatrix} 5.9 & 4.66 & 4.75 & 0 & 0 & 0 \\ 4.66 & 12.85 & 7.8 & 0 & 0 & 0 \\ 4.75 & 7.8 & 12.3 & 0 & 0 & 0 \\ 0 & 0 & 0 & 2.52 & 0 & 0 \\ 0 & 0 & 0 & 0 & 2.26 & 0 \\ 0 & 0 & 0 & 0 & 0 & 1.26 \end{pmatrix}$	Case 2	$\begin{pmatrix} 2.56 & 1.46 & 1.38 & 0 & 0 & 0 \\ 1.46 & 9.15 & 3.9 & 0 & 0 & 0 \\ 1.38 & 3.9 & 7.6 & 0 & 0 & 0 \\ 0 & 0 & 0 & 2.96 & 0 & 0 \\ 0 & 0 & 0 & 0 & 2.12 & 0 \\ 0 & 0 & 0 & 0 & 0 & 1.18 \end{pmatrix}$
Case 3	$\begin{pmatrix} 6.1 & 4.8 & 4.9 & 0 & 0 & 0 \\ 4.8 & 20.3 & 10.7 & 0 & 0 & 0 \\ 4.9 & 10.7 & 18.5 & 0 & 0 & 0 \\ 0 & 0 & 0 & 4.6 & 0 & 0 \\ 0 & 0 & 0 & 0 & 4.14 & 0 \\ 0 & 0 & 0 & 0 & 0 & 2.30 \end{pmatrix}$	Case 4	$\begin{pmatrix} 2.6 & 1.48 & 1.4 & 0 & 0 & 0 \\ 1.48 & 16.4 & 6.5 & 0 & 0 & 0 \\ 1.4 & 6.5 & 13.4 & 0 & 0 & 0 \\ 0 & 0 & 0 & 4.52 & 0 & 0 \\ 0 & 0 & 0 & 0 & 4.06 & 0 \\ 0 & 0 & 0 & 0 & 0 & 2.26 \end{pmatrix}$

**Table 4.** The homogenized stiffness coefficients, in units of MPa.

Case	Hom. elastic and shear moduli (MPa)						Hom. Poisson's ratios		
	$E_1$	$E_2$	$E_3$	$G_{12}$	$G_{23}$	$G_{13}$	$\nu_{12}$	$\nu_{23}$	$\nu_{13}$
1	1.66	7.2	6.7	1.26	1.13	0.63	0.2	0.2	0.25
2	1.54	6.9	5.7	1.48	1.06	0.59	0.1	0.1	0.13
3	1.48	13.3	11.7	2.3	2.07	1.15	0.14	0.14	0.18
4	1.55	13	10.5	2.26	2.03	1.13	0.06	0.06	0.07

**Table 5.** The homogenized elastic moduli and Poisson's ratios.

To the best of our knowledge, there is currently no experimental work available in the literature done on the brain-skull interface region in order to describe its mechanical behavior as a function of the local constituents. In addition, the finite element models of the human head from [Ruan et al. 1993; Zhou et al. 1995; Willinger et al. 1999; Kleiven 2002; Baumgartner and Willinger 2005] all consider the brain-skull interface elements to have isotropic behavior. Therefore, no anisotropic numerical results exist to compare with the current study. In addition, brain injury and head response to impact such as in [Gong et al. 2008; Paka et al. 2011] are always developed on macroscopic models although the behaviors of the different constituents are taken into account. It is therefore clear that intracranial stresses and strains for which safety devices are developed cannot be determined from the influence of these local constituents using these models. However, the methodology used for this analysis is now well established and is based on experimental data available in the literature. A clear anisotropic material behavior is obtained. It can easily be integrated within a 3D macroscopic model (such as a finite element model) in order to study the macroscopic behavior of the brain-skull interface as a function of each local constituent. The influence of the stiffness variations  $E_s$  and  $K_{bl}$  is presented in the next section.

#### 4.2. Influence of external parameter variability.

*Influence of the variation of the superior sagittal sinus Young's modulus  $E_s$ .* As shown in Figure 3, the variation of  $E_s$  leads to nearly linear variations of the homogenized elastic and shear moduli and Poisson's ratio for Case 1. In Figure 3a it can be noticed that the value of the homogenized  $E_1$  remained almost constant and remarkably lower than the values of  $E_2$  and  $E_3$  which increased linearly as functions of  $E_s$ . This behavior is justified by the fact that direction 2 represents the axis of the sinus in the sagittal direction and direction 3 is perpendicular to the SSS and the BV, while direction 1 is that of the BV axis, which is the weakest, and not much affected by the variation of the SSS mechanical properties. On the contrary, the values of the Poisson's ratios (Figure 3b) decreased with the increase of  $E_s$ . The effect of increasing the Young's modulus by a factor of two showed a Poisson's ratio decreasing by a factor of two.

The small results variations shown between the different directions depend on the experimental data used from the literature. On the other hand, the shear moduli increase remarkably as shown in Figure 3c. The observed differences between the different shear moduli are similar to those observed for the Young's moduli. The increase in the SSS stiffness improved the shear resistance of the studied structure in the three planes, which means that the SSS properties control the shear behavior.

*Influence of the variation of the blood equivalent stiffness  $K_{bl}$ .* The variation of the blood equivalent stiffness  $K_{bl}$  also showed a nearly linear variation in all cases as shown in Figure 4 for the homogenized elastic properties (for Case 1). In general, the homogenized properties did not experience remarkable change with the change of  $K_{bl}$ . However the evolution of the RVE Young's moduli follows the same trend as for the variation of ( $E_s$ ). In the same manner, the value of  $E_1$  remains small compared to  $E_2$  and  $E_3$ . On the contrary to the results found with  $E_s$ , the shear moduli are not much affected by the increase of  $K_{bl}$ . However, as opposed to the SSS Young's modulus variation, the Poisson's ratios increase with the increase of  $K_{bl}$  which means that the structure will suffer more Poisson's effect with increasing  $K_{bl}$ .

Regarding the variation of the blood mechanical properties, we can say that it has a limited influence on the overall RVE homogenized mechanical response. This result shows that the influence of the SSS and BVs' walls' stiffness has only a small influence on the mechanical evaluation of the enclosed blood

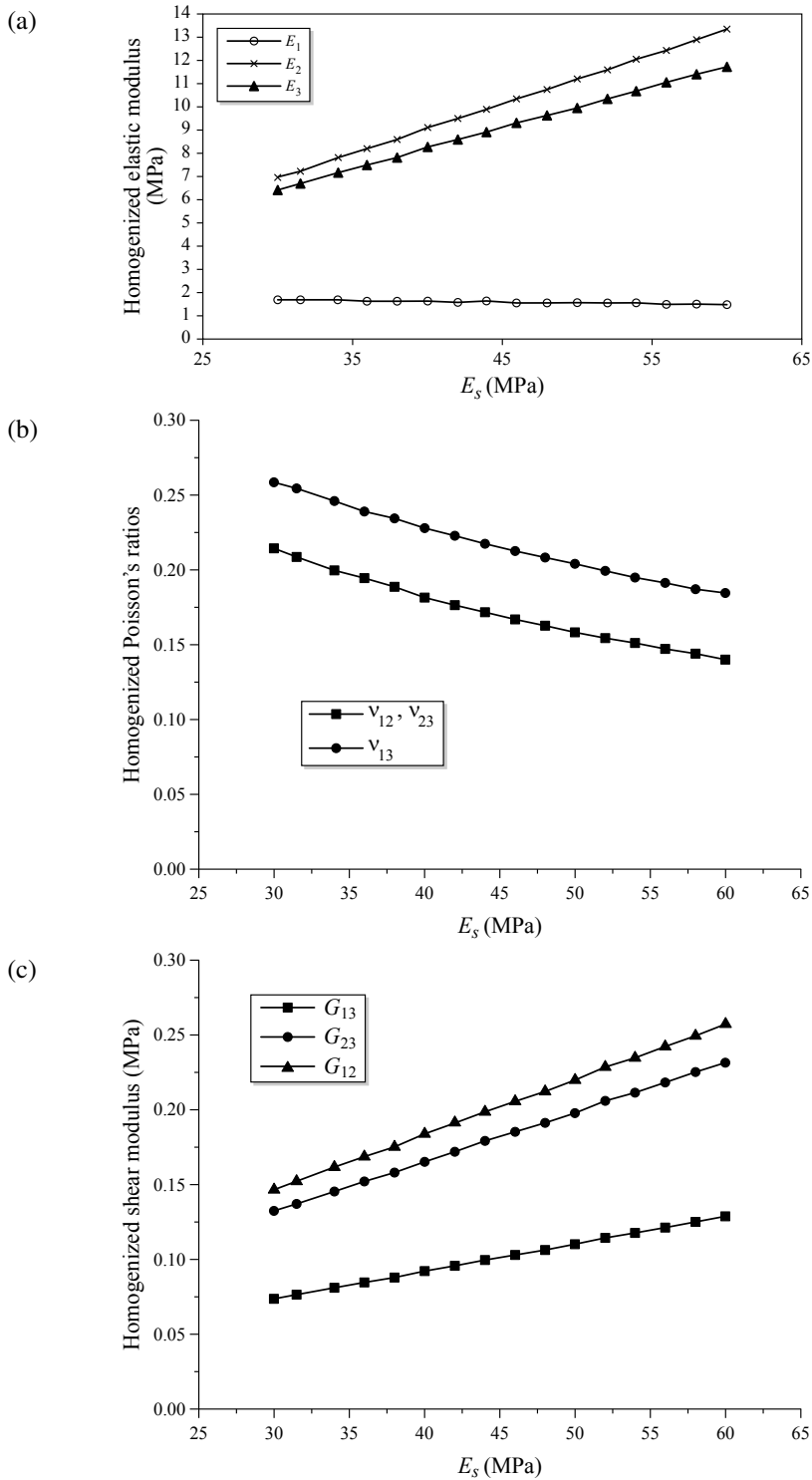


**Figure 3.** Variation of elastic properties of the RVE as a function of  $E_s$ . (a) Elastic modulus. (b) Poisson's ratio. (c) Shear modulus.

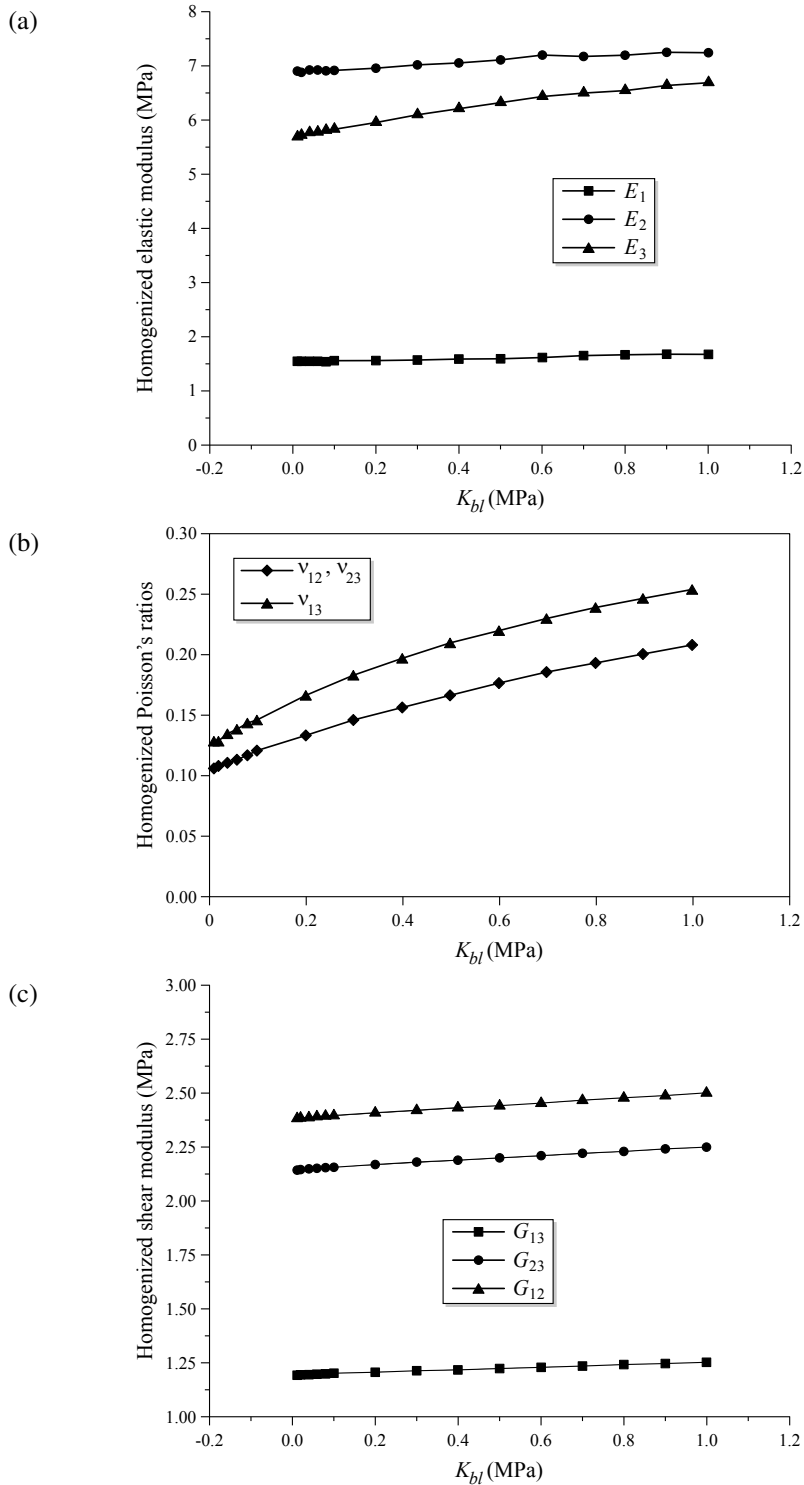


**Figure 4.** Variation of elastic properties with ( $K_{bl}$ ). (a) Elastic modulus. (b) Poisson's ratio. (c) Shear modulus.

mechanical response. The homogenized RVE response will not be much influenced by the blood properties but instead mainly by the constituents’ mechanical behavior. In addition, note that all mechanical characteristics are currently linear elastic. It is expected that using a more complex material response (nonlinear) may have an impact on the homogenized RVE properties as well as on the overall mechanical response.

### 5. Conclusion

The distribution of bridging veins (BVs) being almost periodic along the superior sagittal sinus (SSS) in the sagittal plane, we used the homogenization technique based on asymptotic expansion at the mesoscale. This enabled us to calculate the effective anisotropic elastic properties of the brain-skull interface region. The considered representative volume element (RVE) contains the sinus, the BVs, the blood, and the surrounding brain-skull interface region and tissues. The homogenized stiffness tensor was calculated and showed a high degree of anisotropy. In addition, the effect of the variation of the tissues’ mechanical properties was also studied. The variation of the SSS elastic modulus had an important impact on the effective properties whereas the variability of the blood properties showed a limited effect. This investigation showed its interest in the predictability of the local mechanical response of the brain-skull interface region and the SSS-BV compound in particular when using modern computerized methods. The obtained results for the RVE properties can be implemented in a macroscopic model such as a FEM to study head injury problems.

### Appendix

Here, we give the expressions of the calculated effective rigidity coefficients for the considered RVE as a function of the local constituents’ properties. We recall that the case was presented earlier for the evaluation of the coefficient  $K_{44}^*$  in (29) using  $r, s = (2, 3)$  and (24).

For solving the coefficients  $K_{55}^*$  and  $K_{66}^*$ , we used the same methodology as previously described and obtained the corresponding coefficients as:

(1) For  $r, s = (1, 3)$  and (25):

$$W_2^*(M) = \{ \sigma / \sigma_{11} = 0|_{0,L_1}; \sigma_{21} = \sigma_{23} = 0|_{0,L_2}; \sigma_{33} = 0|_{0,L_3} \},$$

we get:

$$K_{55}^* = 2G_{13}^* = \frac{1}{\frac{3}{8} K_{55BSIR}^{-1} + \frac{1}{14.4} K_{55BV}^{-1} + \frac{1}{2.9} K_{55bl}^{-1} + \frac{1}{4.7} K_{55SS}^{-1}}. \tag{A.1}$$

(2) For  $r, s = (1, 2)$  and (26):

$$W_3^*(M) = \{ \sigma / \sigma_{11} = 0|_{0,L_1}; \sigma_{22} = 0|_{0,L_2}; \sigma_{31} = \sigma_{32} = 0|_{0,L_3} \},$$

we get:

$$K_{66}^* = 2G_{12}^* = \frac{1}{\frac{3}{8} K_{66BSIR}^{-1} + \frac{1}{14.4} K_{66BV}^{-1} + \frac{1}{2.9} K_{66bl}^{-1} + \frac{1}{4.7} K_{66SS}^{-1}}. \tag{A.2}$$

We note the equations are identical  $K_{44}^* = K_{55}^* = K_{66}^*$  but anisotropic behavior comes from the different material characteristics in the different directions.

In the cases of  $K_{11}^*$ ,  $K_{12}^*$ ,  $K_{13}^*$ ,  $K_{22}^*$ ,  $K_{23}^*$ , and  $K_{33}^*$ , the problem is more difficult to solve. We are presenting here the general methodology used in the case of  $r, s = (1, 1)$  presented in (19) and obtaining the other coefficients follows the same resolution process. We recall that the RVE is subdivided into 64 subportions taking into account the 3D symmetries and each part of the different materials studied and present within the RVE. When replacing the mechanical characteristics of each constituent in (19) and isolating the terms associated with each  $\epsilon_{11}^*$ ,  $\epsilon_{22}^*$ , and  $\epsilon_{33}^*$  we obtained a set of three equations given by

$$\begin{aligned} & \left( \frac{3}{8} K_{11\text{BSIR}} + \frac{1}{14.4} K_{11\text{BV}} + \frac{1}{2.9} K_{11\text{bl}} + \frac{1}{4.7} K_{11\text{SS}} \right) a \\ & + \left( -\frac{1}{8} K_{12\text{BSIR}} + \frac{1}{14.4} K_{12\text{BV}} + \frac{1}{21.6} K_{12\text{bl}} + \frac{1}{108} K_{12\text{SS}} \right) b \\ & + \left( \frac{1}{8} K_{13\text{BSIR}} - \frac{1}{14.4} K_{13\text{BV}} + \frac{1}{10.8} K_{13\text{bl}} - \frac{1}{6.75} K_{13\text{SS}} \right) c \\ & + \left( -\frac{3}{8} K_{11\text{BSIR}} - \frac{1}{14.4} K_{11\text{BV}} + \frac{1}{4.32} K_{11\text{bl}} + \frac{1}{4.7} K_{11\text{SS}} \right) = 0, \quad (\text{A.3}) \end{aligned}$$

$$\begin{aligned} & \left( -\frac{1}{8} K_{12\text{BSIR}} + \frac{1}{14.4} K_{12\text{BV}} + \frac{1}{21.6} K_{12\text{bl}} + \frac{1}{108} K_{12\text{SS}} \right) a \\ & + \left( \frac{3}{8} K_{22\text{BSIR}} + \frac{1}{14.4} K_{22\text{BV}} + \frac{1}{2.9} K_{22\text{bl}} + \frac{1}{4.7} K_{22\text{SS}} \right) b \\ & + \left( \frac{1}{8} K_{23\text{BSIR}} - \frac{1}{14.4} K_{23\text{BV}} - \frac{1}{15.4} K_{23\text{bl}} + \frac{1}{108} K_{23\text{SS}} \right) c \\ & + \left( \frac{1}{8} K_{12\text{BSIR}} - \frac{1}{14.4} K_{12\text{BV}} - \frac{1}{15.4} K_{12\text{bl}} + \frac{1}{108} K_{12\text{SS}} \right) = 0, \quad (\text{A.4}) \end{aligned}$$

$$\begin{aligned} & \left( \frac{1}{8} K_{13\text{BSIR}} - \frac{1}{14.4} K_{13\text{BV}} + \frac{1}{10.8} K_{13\text{bl}} - \frac{1}{6.75} K_{13\text{SS}} \right) a \\ & + \left( \frac{1}{8} K_{23\text{BSIR}} - \frac{1}{14.4} K_{23\text{BV}} - \frac{1}{15.4} K_{23\text{bl}} + \frac{1}{108} K_{23\text{SS}} \right) b \\ & + \left( \frac{3}{8} K_{33\text{BSIR}} + \frac{1}{14.4} K_{33\text{BV}} + \frac{1}{2.9} K_{33\text{bl}} + \frac{1}{4.7} K_{33\text{SS}} \right) c \\ & + \left( -\frac{1}{8} K_{13\text{BSIR}} + \frac{1}{14.4} K_{13\text{BV}} + \frac{1}{4.9} K_{13\text{bl}} - \frac{1}{6.75} K_{13\text{SS}} \right) = 0, \quad (\text{A.5}) \end{aligned}$$

where the subscripts BSIR, BV, bl, and SSS indicate the cerebrospinal fluid, bridging vein, blood, and superior sagittal sinus, respectively. The parameters  $a$ ,  $b$ , and  $c$  are the given boundary conditions at the RVE's symmetries and each materials' subportions. They take the values  $\epsilon_1$ ,  $\epsilon_2$ , and  $\epsilon_3$  depending on each subportion boundary condition of the RVE and the axis directions. The constants  $a$ ,  $b$ , and  $c$  are evaluated when solving the system of three equations above as a function of the material parameters, and the effective stiffness coefficients can be obtained from (20), (21), and (22) so that

$$\begin{aligned} K_{11}^* & = \left( -\frac{3}{8} K_{11\text{BSIR}} - \frac{1}{14.4} K_{11\text{BV}} + \frac{1}{4.32} K_{11\text{bl}} + \frac{1}{4.7} K_{11\text{SS}} \right) a \\ & + \left( \frac{1}{8} K_{12\text{BSIR}} - \frac{1}{14.4} K_{12\text{BV}} - \frac{1}{15.4} K_{12\text{bl}} + \frac{1}{108} K_{12\text{SS}} \right) b \\ & + \left( -\frac{1}{8} K_{13\text{BSIR}} + \frac{1}{14.4} K_{13\text{BV}} + \frac{1}{4.9} K_{13\text{bl}} - \frac{1}{6.75} K_{13\text{SS}} \right) c \\ & + \left( \frac{3}{8} K_{11\text{BSIR}} + \frac{1}{14.4} K_{11\text{BV}} + \frac{1}{2.9} K_{11\text{bl}} + \frac{1}{4.7} K_{11\text{SS}} \right), \quad (\text{A.6}) \end{aligned}$$

$$\begin{aligned}
 K_{21}^* = & \left(-\frac{3}{8}K_{12BSIR} - \frac{1}{14.4}K_{12BV} + \frac{1}{4.32}K_{12bl} + \frac{1}{4.7}K_{12SS}\right)a \\
 & + \left(\frac{1}{8}K_{22BSIR} - \frac{1}{14.4}K_{22BV} - \frac{1}{15.4}K_{22bl} + \frac{1}{108}K_{22SS}\right)b \\
 & + \left(-\frac{1}{8}K_{23BSIR} + \frac{1}{14.4}K_{23BV} + \frac{1}{4.9}K_{23bl} - \frac{1}{6.75}K_{23SS}\right)c \\
 & + \left(\frac{3}{8}K_{12BSIR} + \frac{1}{14.4}K_{12BV} + \frac{1}{2.9}K_{12bl} + \frac{1}{4.7}K_{12SS}\right), \quad (A.7)
 \end{aligned}$$

$$\begin{aligned}
 K_{31}^* = & \left(-\frac{3}{8}K_{13BSIR} - \frac{1}{14.4}K_{13BV} + \frac{1}{4.32}K_{13bl} + \frac{1}{4.7}K_{13SS}\right)a \\
 & + \left(\frac{1}{8}K_{23BSIR} - \frac{1}{14.4}K_{23BV} - \frac{1}{15.4}K_{23bl} + \frac{1}{108}K_{23SS}\right)b \\
 & + \left(-\frac{1}{8}K_{33BSIR} + \frac{1}{14.4}K_{33BV} + \frac{1}{4.9}K_{33bl} - \frac{1}{6.75}K_{33SS}\right)c \\
 & + \left(\frac{3}{8}K_{13BSIR} + \frac{1}{14.4}K_{13BV} + \frac{1}{2.9}K_{13bl} + \frac{1}{4.7}K_{13SS}\right). \quad (A.8)
 \end{aligned}$$

In a similar way, we solve the problem for  $r, s = (2, 2)$  and  $r, s = (3, 3)$ . The general equations are given by

$$\begin{aligned}
 \sum_{i=1}^8 \int_i \{ & (K_{11}\epsilon_{11} + K_{12}\epsilon_{22} + K_{13}\epsilon_{33})\epsilon_{11}^* + (K_{21}\epsilon_{11} + K_{22}\epsilon_{22} + K_{23}\epsilon_{33})\epsilon_{22}^* + (K_{31}\epsilon_{11} + K_{32}\epsilon_{22} + K_{33}\epsilon_{33})\epsilon_{33}^* \\
 & + (K_{21}\epsilon_{11}^* + K_{22}\epsilon_{22}^* + K_{23}\epsilon_{33}^*)dV_i \} = 0, \quad \forall \epsilon_{11}^*, \epsilon_{22}^*, \epsilon_{33}^* \in W_0(M), \quad (A.9)
 \end{aligned}$$

$$\begin{aligned}
 \sum_{i=1}^8 \int_i \{ & (K_{11}\epsilon_{11} + K_{12}\epsilon_{22} + K_{13}\epsilon_{33})\epsilon_{11}^* + (K_{21}\epsilon_{11} + K_{22}\epsilon_{22} + K_{23}\epsilon_{33})\epsilon_{22}^* + (K_{31}\epsilon_{11} + K_{32}\epsilon_{22} + K_{33}\epsilon_{33})\epsilon_{33}^* \\
 & + (K_{31}\epsilon_{11}^* + K_{32}\epsilon_{22}^* + K_{33}\epsilon_{33}^*)dV_i \} = 0, \quad \forall \epsilon_{11}^*, \epsilon_{22}^*, \epsilon_{33}^* \in W_0(M), \quad (A.10)
 \end{aligned}$$

and we find the resulting equations with the relations  $K_{11}^* = K_{22}^* = K_{33}^*$  and  $K_{12}^* = K_{13}^* = K_{23}^*$ . The anisotropic behavior is again given by the different material characteristics in different directions.

Lastly, the effective stiffness matrix is given for an orthotropic material with

$$K_{ijkl}^* = \begin{pmatrix} K_{11}^* & K_{12}^* & K_{13}^* & 0 & 0 & 0 \\ K_{12}^* & K_{22}^* & K_{23}^* & 0 & 0 & 0 \\ K_{13}^* & K_{23}^* & K_{33}^* & 0 & 0 & 0 \\ 0 & 0 & 0 & K_{44}^* & 0 & 0 \\ 0 & 0 & 0 & 0 & K_{55}^* & 0 \\ 0 & 0 & 0 & 0 & 0 & K_{66}^* \end{pmatrix}. \quad (A.11)$$

After calculating the effective stiffness coefficients using the local material characteristics and the matrix (A.11), we can obtain the results presented in Table 4.

### References

[Bashkatov et al. 2003] A. N. Bashkatov, E. A. Genina, Y. P. Sinichkin, V. I. Kochubey, N. A. Lakodina, and V. V. Tuchin, “Glucose and mannitol diffusion in human dura mater”, *Biophys. J.* **85** (2003), 3310–3318.

[Baumgartner and Willinger 2005] D. Baumgartner and R. Willinger, “Human head tolerance limits to specific injury mechanisms inferred from real world accident numerical reconstruction”, *Rev. Eur. Élé. Finis* **14**:4-5 (2005), 421–444.

- [Bayly et al. 2005] P. V. Bayly, T. S. Cohen, E. P. Leister, D. Ajo, E. C. Leuthardt, and G. M. Genin, “Deformation of the human brain induced by mild acceleration”, *J. Neurotrauma* **22**:8 (2005), 845–856.
- [Bertaud et al. 2010] J. Bertaud, Z. Qin, and M. J. Buehler, “Intermediate filament-deficient cells are mechanically softer at large deformation: a multiscale simulation study”, *Acta Biomater.* **6** (2010), 2457–2466.
- [Bloomfield et al. 1998] I. G. Bloomfield, I. H. Johnston, and L. E. Bilston, “Effects of proteins, blood cells and glucose on the viscosity of cerebrospinal fluid”, *Pediatr. Neurosurg.* **28**:5 (1998), 246–251.
- [Chatziprodromou et al. 2007] I. Chatziprodromou, A. Tricoli, D. Poulikakos, and Y. Ventikos, “Haemodynamics and wall remodeling of a growing cerebral aneurysm : a computational model”, *J. Biomech.* **40**:2 (2007), 412–426.
- [Delye et al. 2006] H. Delye, J. Goffin, P. Verschueren, J. V. Sloten, G. Van Der Perre, H. Alaerts, I. Verpoest, and D. Berckmans, “Biomechanical properties of the superior sagittal sinus-bridging vein complex”, *Stapp Car Crash J.* **50** (2006), 625–636.
- [Devries et al. 1989] F. Devries, H. Dumontet, G. Duvaut, and F. L  n  , “Homogenization and damage for composite structures”, *Int. J. Numer. Methods Eng.* **27**:2 (1989), 285–298.
- [Dumont et al. 1987] J. P. Dumont, P. Ladeveze, M. Poss, and Y. R  mond, “Damage mechanics for 3-D composites”, *Compos. Struct.* **8**:2 (1987), 119–141.
- [Fenderson et al. 2007] B. A. Fenderson, R. Rubin, and E. Rubin, *Lippincott’s review of pathology: illustrated interactive Q & A*, Lippincott Williams and Wilkins, Philadelphia, 2007.
- [Gong et al. 2008] S. W. Gong, H. P. LEE, and C. Lu, “Computational simulation of the human head response to non-contact impact”, *Comput. Struct.* **86** (2008), 758–770.
- [Henrikson et al. 1997] R. C. Henrikson, G. I. Kaye, and J. E. Mazurkiewicz, *Histology*, National Medical Series for Independent Study, Lippincott Williams and Wilkins, Baltimore, 1997.
- [Ho and Kleiven 2007] J. Ho and S. Kleiven, “Dynamic response of the brain with vasculature: a three-dimensional computational study”, *J. Biomech.* **40**:13 (2007), 3006–3012.
- [Horgan 2005] T. J. Horgan, *A finite element model of the human head for use in the study of pedestrian accident*, PhD thesis, National University of Ireland, Dublin, 2005.
- [Huang et al. 1999] Y. Huang, M. C. Lee, W. T. Chiu, C. T. Chen, and S. Y. Lee, “Three-dimensional finite element analysis of subdural hematoma”, *J. Trauma* **47** (1999), 538–544.
- [Ji and Margulies 2007] S. Ji and S. S. Margulies, “In vivo pons motion within the skull”, *J. Biomech.* **40** (2007), 92–99.
- [Ji et al. 2004] S. Ji, Q. Zhu, L. Dougherty, and S. S. Margulies, “In vivo measurements of human brain displacement”, *Stapp Car Crash J.* **48** (2004), 227–237.
- [Karami et al. 2009] G. Karami, N. Grundman, N. Abolfathi, A. Naik, and M. Ziejewski, “A micromechanical hyperelastic modeling of brain white matter under large deformation”, *J. Mech. Behav. Biomed. Mater.* **2** (2009), 243–254.
- [Kleiven 2002] S. Kleiven, *Finite element modeling of the human head*, PhD thesis, Royal Institute of Technology, Stockholm, 2002.
- [Kleiven and Hardy 2002] S. Kleiven and W. N. Hardy, “Correlation of a finite element model of human head with local brain motion: consequences for injury prediction”, *Stapp Car Crash J.* **46** (2002), 123–144.
- [Kumaresan and Radhakrishnan 1996] S. Kumaresan and S. Radhakrishnan, “Importance of partitioning membranes of the brain and the influence of the neck in head injury modeling”, *Med. Biol. Eng. Comput.* **34**:1 (1996), 27–32.
- [Ladeveze et al. 1985] P. Ladeveze, L. Proslier, and Y. R  mond, “Reconstruction of a 3-D composite behaviour from a local approach”, pp. 1025–1037 in *Fifth International Conference on Composite Materials (ICCM-V)*, vol. 5, edited by W. C. Harrigan et al., 1985.
- [Lee and Haut 1989] M. C. Lee and R. C. Haut, “Insensitivity of tensile failure properties of human bridging veins to strain rate: implication in biomechanics of subdural hematoma”, *J. Biomech.* **22**:6-7 (1989), 537–542.
- [Li et al. 2007] M. X. Li, J. J. Beech-Brandt, L. R. John, P. R. Hoskins, and W. J. Easson, “Numerical analysis of pulsatile blood flow and vessel wall mechanics in different degrees of stenosis”, *J. Biomech.* **40**:16 (2007), 3715–3724.
- [Mahmoud 2010] R. A. R. Mahmoud, *Towards the building of a local criteria of vascular lesion at the microscopical scale using homogenization*, Ph.D. thesis, Institut de M  canique des Fluides et des Solides, Universit   de Strasbourg, 2010.

- [Maxeiner and Wolff 2002] H. Maxeiner and M. Wolff, “Pure subdural hematomas: a postmortem analysis of their form and bleeding points”, *Neurosurg.* **50**:3 (2002), 503–509.
- [Melvin et al. 1970] J. W. Melvin, J. H. McElhaney, and V. L. Roberts, “Development of a mechanical model of the human head: determination of tissue properties and synthetic substitute materials”, Technical report SAE Paper No. 700903, University of Michigan/Society of Automobile Engineers, 1970.
- [Moghadam and Sadegh 2009] M. Z. Moghadam and A. M. Sadegh, “Global/local head models to analyze cerebral blood vessel rupture leading to ASDH and SAH”, *Comput. Methods Biomech. Biomed. Engin.* **12**:1 (2009), 1–12.
- [Monson et al. 2005] K. L. Monson, W. Goldsmith, N. M. Barbaro, and G. T. Manley, “Significant of source and size in the mechanical response of human cerebral blood vessels”, *J. Biomech.* **38** (2005), 737–744.
- [Mukherjee et al. 2006] S. Mukherjee, A. Chawla, and B. Karthikeyan, “A review of the mechanical properties of human body soft tissues in the head, neck and spine”, *Inst. Eng. J.* **87** (2006), 10–24.
- [Paka et al. 2011] P. Paka, G. Karami, and M. Ziejewski, “Examination of brain injury under impact with the ground of various stiffness”, *Proc. Eng.* **13** (2011), 409–414.
- [Park and Lakes 2007] J. B. Park and R. S. Lakes, *Biomaterials: an introduction*, 3rd ed., pp. 245–247, Springer, New York, 2007, Available at <http://www.springerlink.com/content/978-0-387-37879-4>.
- [Pham and Sun 2010] T. Pham and W. Sun, “Characterization of the mechanical properties of the coronary sinus for percutaneous transvenous mitral annuloplasty”, *Acta Biomater.* **6** (2010), 4336–4344.
- [Prevost et al. 2011a] T. P. Prevost, A. Balakrishnan, S. Suresh, and S. Socrate, “Biomechanics of brain tissues”, *Acta Biomater.* **7** (2011), 83–95.
- [Prevost et al. 2011b] T. P. Prevost, G. Jin, M. A. de Moya, H. B. Alam, S. Suresh, and S. Socrate, “Dynamic mechanical response of brain tissue in indentation in vivo, in situ and in vitro”, *Acta Biomater.* **7** (2011), 4090–4101.
- [Rhoton 2002] A. L. Rhoton, Jr., “The cerebral veins”, *Neurosurg.* **51**:Supplement 1 (2002), 159–205.
- [Ruan and Prasad 1996] J. S. Ruan and P. Prasad, “Study of the biodynamic characteristics of the human head”, pp. 63–74 in *1996 International Conference on the Biomechanics of Impacts* (Dublin, 1996), edited by D. Césari and A. Charpenne, IRCOBI, Bron, 1996.
- [Ruan et al. 1991] J. S. Ruan, T. B. Khalil, and A. I. King, “Human head impact dynamic response to side impact by finite element modeling”, *J. Biomech. Eng. (ASME)* **113** (1991), 276–283.
- [Ruan et al. 1993] J. S. Ruan, T. B. Khalil, and A. I. King, “Finite element modeling of direct head impact”, Technical report SAE Paper No. 933114, Wayne State University/Society of Automobile Engineers, 1993.
- [Sabet et al. 2008] A. A. Sabet, E. Christoforou, B. Zatlin, G. M. Genin, and P. V. Bayly, “Deformation of the human brain induced by mild angular head acceleration”, *J. Biomech.* **41** (2008), 307–315.
- [Samet and Lelkes 1999] M. M. Samet and P. I. Lelkes, “The hemodynamic environment of endothelium in vivo and its simulation in vitro”, pp. 8–9 in *Mechanical forces and the endothelium*, edited by P. L. Lelkes, Endothelial Cell Research Series **6**, Harwood, Amsterdam, 1999.
- [Sanchez-Palencia 1974] E. Sanchez-Palencia, “Comportement local et macroscopique d’un type de milieux physiques hétérogènes”, *Int. J. Eng. Sci.* **12**:4 (1974), 331–351.
- [Sanz-Herrera et al. 2009] J. A. Sanz-Herrera, J. M. Garcia-Aznar, and M. Doblaré, “On scaffold designing for bone regeneration: a computational multiscale approach”, *Acta Biomater.* **5**:1 (2009), 219–229.
- [Sarkar et al. 2004] S. Sarkar, S. Majumder, and A. Roychowdhury, “Response of human head under static and dynamic load using finite element method”, *Trend. Biomater. Artif. Organ.* **17**:2 (2004), 130–134.
- [Soliman et al. 2010] S. Soliman, S. Pagliari, A. Rinaldi, G. Forte, R. Fiaccavento, F. Pagliari, O. Franzese, M. Minieri, P. Di Nardo, S. Liccocia, and E. Traversa, “Multiscale three-dimensional scaffolds for soft tissue engineering via multimodal electrospinning”, *Acta Biomater.* **6** (2010), 1227–1237.
- [Vignes et al. 2007] J.-R. Vignes, A. Dagain, D. Liguoro, and J. Guérin, “A hypothesis of cerebral venous system regulation based on a study of the junction between the cortical bridging veins and the superior sagittal sinus”, *J. Neurosurg.* **107** (2007), 1205–1210.

- [Willinger and Césari 1990] R. Willinger and D. Césari, “Determination of cerebral motion at impact through mechanical impedance methods”, pp. 203–214 in *1990 International Conference on the Biomechanics of Impacts* (Bron-Lyon, 1990), edited by D. Césari and A. Charpenne, IRCOBI, Bron, 1990.
- [Willinger et al. 1992] R. Willinger, C. M. Kopp, and D. Césari, “New concept of contrecoup lesion mechanism: modal analysis of a finite element head model”, pp. 283–297 in *1992 International Conference on the Biomechanics of Impacts* (Verona, 1992), edited by D. Césari and A. Charpenne, IRCOBI, Bron, 1992.
- [Willinger et al. 1995] R. Willinger, L. Taleb, and C. M. Kopp, “Modal and temporal analysis of head mathematical models”, *J. Neurotrauma* **12**:4 (1995), 743–754.
- [Willinger et al. 1999] R. Willinger, H. S. Kang, and B. M. Diaw, “Three dimensional human head finite element model validation against experimental impacts”, *Ann. Biomed. Eng.* **27**:3 (1999), 403–410.
- [Wittek and Omori 2003] A. Wittek and K. Omori, “Parametric study of effects of brain-skull boundary conditions and brain material properties on responses of simplified finite element brain model under angular acceleration impulse in sagittal plane”, *Trans. Jpn. Soc. Mech. Eng. C* **46**:4 (2003), 1388–1399.
- [Yamashima and Friede 1984] T. Yamashima and R. L. Friede, “Why do bridging veins rupture in the virtual subdural space?”, *J. Neurol. Neurosurg. Psychiatry* **47** (1984), 121–127.
- [Yao et al. 2008] J. Yao, J. Yang, and D. Otte, “Investigation of head injuries by reconstruction of real world vehicles-versus-adult-pedestrian accidents”, *Saf. Sci.* **46**:7 (2008), 1103–1114.
- [Yoon et al. 2002] Y. J. Yoon, G. Yang, and S. C. Cowin, “Estimation of the effective transversely isotropic elastic constants of a material from known values of the material’s orthotropic elastic constants”, *Biomech. Model. Mechanobiol.* **1** (2002), 83–93.
- [Yu et al. 2008] X. Yu, L. Wang, S. Sun, and L. Tong, “Viscoelastic finite element analysis of human skull-dura mater system as intracranial pressure changing”, *Afr. J. Biotechnol.* **7**:6 (2008), 689–695.
- [Zhou et al. 1995] C. Zhou, T. B. Khalil, and A. I. King, “A new model comparing impact responses of the homogeneous and inhomogeneous human brain”, Technical Report SAE Paper No. 952714, Wayne State University/Society of Automobile Engineers, 1995.

Received 11 May 2012. Revised 25 Jul 2012. Accepted 25 Jul 2012.

RANIA ABDEL RAHMAN: [rania.elanwar@gmail.com](mailto:rania.elanwar@gmail.com)

Faculty of Engineering, The French University of Egypt, BP 21 Chorouk city, Km 37, Highway Cairo-Ismailia, Egypt

DANIEL GEORGE: [george@unistra.fr](mailto:george@unistra.fr)

Institute of Fluids and Solid Mechanics, University of Strasbourg / CNRS, 2 rue Boussingault, 67000 Strasbourg, France

DANIEL BAUMGARTNER: [daniel.baumgartner@unistra.fr](mailto:daniel.baumgartner@unistra.fr)

Institute of Fluids and Solid Mechanics, University of Strasbourg/CNRS, 2 rue Boussingault, 67000 Strasbourg, France

MATHIEU NIERENBERGER: [mathieu.nierenberger@etu.unistra.fr](mailto:mathieu.nierenberger@etu.unistra.fr)

Institute of Fluids and Solid Mechanics, University of Strasbourg/CNRS, 2 rue Boussingault, 67000 Strasbourg, France

YVES RÉMOND: [remond@unistra.fr](mailto:remond@unistra.fr)

Institute of Fluids and Solid Mechanics, University of Strasbourg/CNRS, 2 rue Boussingault, 67000 Strasbourg, France

SAÏD AHZI: [ahzi@unistra.fr](mailto:ahzi@unistra.fr)

Institute of Fluid and Solid Mechanics UMR, University of Strasbourg/CNRS, 2 Rue Boussingault, 67000 Strasbourg, France

# JOURNAL OF MECHANICS OF MATERIALS AND STRUCTURES

[jomms.net](http://jomms.net)

Founded by Charles R. Steele and Marie-Louise Steele

## EDITORS

CHARLES R. STEELE Stanford University, USA  
DAVIDE BIGONI University of Trento, Italy  
IWONA JASIUK University of Illinois at Urbana-Champaign, USA  
YASUHIRO SHINDO Tohoku University, Japan

## EDITORIAL BOARD

H. D. BUI École Polytechnique, France  
J. P. CARTER University of Sydney, Australia  
R. M. CHRISTENSEN Stanford University, USA  
G. M. L. GLADWELL University of Waterloo, Canada  
D. H. HODGES Georgia Institute of Technology, USA  
J. HUTCHINSON Harvard University, USA  
C. HWU National Cheng Kung University, Taiwan  
B. L. KARIHALOO University of Wales, UK  
Y. Y. KIM Seoul National University, Republic of Korea  
Z. MROZ Academy of Science, Poland  
D. PAMPLONA Universidade Católica do Rio de Janeiro, Brazil  
M. B. RUBIN Technion, Haifa, Israel  
A. N. SHUPIKOV Ukrainian Academy of Sciences, Ukraine  
T. TARNAI University Budapest, Hungary  
F. Y. M. WAN University of California, Irvine, USA  
P. WRIGGERS Universität Hannover, Germany  
W. YANG Tsinghua University, China  
F. ZIEGLER Technische Universität Wien, Austria

**PRODUCTION** [contact@msp.org](mailto:contact@msp.org)

SILVIO LEVY Scientific Editor

Cover design: Alex Scorpan

Cover photo: Ev Shafir

See <http://jomms.net> for submission guidelines.

JoMMS (ISSN 1559-3959) is published in 10 issues a year. The subscription price for 2012 is US\$555/year for the electronic version, and \$735/year (+ \$60 shipping outside the US) for print and electronic. Subscriptions, requests for back issues, and changes of address should be sent to Mathematical Sciences Publishers, Department of Mathematics, University of California, Berkeley, CA 94720–3840.

JoMMS peer-review and production is managed by EditFLOW<sup>®</sup> from Mathematical Sciences Publishers.

PUBLISHED BY  
 **mathematical sciences publishers**  
<http://msp.org/>

A NON-PROFIT CORPORATION

Typeset in L<sup>A</sup>T<sub>E</sub>X

Copyright ©2012 by Mathematical Sciences Publishers

- The implicit corotational method and its use in the derivation of nonlinear structural models for beams and plates**  
GIOVANNI GARCEA, ANTONIO MADEO and RAFFAELE CASCIARO 509
- Nonlinear FEM analysis for beams and plate assemblages based on the implicit corotational method**  
GIOVANNI GARCEA, ANTONIO MADEO and RAFFAELE CASCIARO 539
- Damage development in an armor alumina impacted with ductile metal spheres**  
BRETT G. COMPTON, ELEANOR A. GAMBLE, VIKRAM S. DESHPANDE and FRANK W. ZOK 575
- An asymptotic method for the prediction of the anisotropic effective elastic properties of the cortical vein: superior sagittal sinus junction embedded within a homogenized cell element**  
RANIA ABDEL RAHMAN, DANIEL GEORGE, DANIEL BAUMGARTNER, MATHIEU NIERENBERGER, YVES RÉMOND and SAÏD AHZI 593